Jurnal Kejuruteraan 38(7) 2026: 3349-3364
https://doi.org/10.17576/jkukm-2026-38(7)-15

Integrated Experimental and Hybrid CFD–ANN Analysis of Transient Cooling Behaviour in Jet Mixing Systems for Reactor Thermal Stability

Nadia Kamarrudin[a,b], Masli Irwan Rosli[b*], Mohd Sobri Takriff[c], Muhammad Shafiq Mat Shayuti[a], Nur Tantiyani Ali Othman[b] & Khairul Naim Ahmad[b]

[a]*Faculty of Chemical Engineering, Universiti Teknologi MARA (UiTM), Shah Alam 40450, Malaysia*

[b]*Faculty of Engineering and Built Environment, Universiti Kebangsaan Malaysia, 43600 Bandar Baru Bangi Selangor Malaysia*

[c]*Chemical and Water Desalination Engineering Program, College of Engineering, University of Sharjah, United Arab Emirates*

[*]*Corresponding author: masli@ukm.edu.my*

Received 4 March 2026, Received in revised form 7 July 2026
Accepted 7 August 2026, Available online 30 October 2026

ABSTRACT

Efficient heat removal is essential for maintaining thermal stability and operational safety in chemical reactors and mixing vessels. This study investigates the transient cooling performance of a jet mixing reactor system using an integrated experimental, Computational Fluid Dynamics (CFD), and Artificial Neural Network (ANN) modelling approach. Experiments were conducted in a cylindrical stainless-steel reactor using water as the working fluid at a Reynolds number of Re = 4300 for two jet configurations (45° side jet and a 90° axial bottom jet). The validated CFD model was then employed to explore six jet configurations, including side jets at 5°, 25°, 45°, and 65°, as well as axial jets at 90° injected from the bottom and top of the reactor. Cooling performance was quantified using normalised temperature decay and two characteristic cooling indicators, t_{50} (time at 50% cooling) and t_{90} (time at 90% cooling). The results show that jet orientation significantly affects cooling efficiency. The 90° axial jet top side achieved the best performance with t_{50} = 325 s and t_{90} = 1051 s, improving cooling time by approximately 14–16% compared with the worst configuration (5° side jet). An ANN surrogate model trained using CFD-generated data achieved mean square error (MSE) on the order of 10^{-8}, demonstrating high predictive accuracy within the parameter ranges. The integrated experimental and hybrid CFD–ANN framework provides an efficient tool for analysing and optimising jet-induced cooling systems in reactor applications for thermal management strategies.

Keywords: Artificial Neural Network (ANN); Computational Fluid Dynamics (CFD); cooling performance indicators; jet mixing cooling; transient heat transfer

INTRODUCTION

Thermal management in chemical reactors and mixing vessels is a critical determinant of process safety, operational reliability, and product quality. In industrial sectors such as chemical manufacturing, pharmaceuticals, and energy systems, uncontrolled heat accumulation from exothermic reactions can lead to severe hazards, including thermal runaway, equipment failure, and catastrophic incidents (Chen et al. 2021; Rossi et al. 2015; Yang et al. 2024). The increasing complexity of modern processing systems, coupled with the push toward intensified and sustainable operations, has boosted the need for robust and responsive cooling strategies (Balasubramanian et al. 2003; Liu & Wilhite 2022).

Among various cooling techniques, jet mixing has emerged as a promising approach due to its ability to enhance convective heat transfer through forced circulation and turbulence generation (Dakshinamoorthy et al. 2006). Chen et al. (2022) revealed that jet mixing produces complex flow structures that promote rapid redistribution of thermal energy when a cooling fluid is injected into the

reactor at controlled velocities and orientations. The effectiveness of jet mixing is governed by multiple interacting parameters, including jet velocity, injection angle, nozzle geometry, and fluid properties (Dakshinamoorthy et al. 2006; Torré et al. 2008). In particular, the hydrodynamic features generated by jet injection, such as vortices, recirculation zones, and turbulent eddies, play a central role in determining the rate and uniformity of heat removal. However, the transient nature of these processes, coupled with their three dimensional and nonlinear characteristics, makes their analysis inherently challenging (Liu & Wilhite 2022; Torré et al. 2007).

Extensive research has been conducted on jet mixing in reactor systems, demonstrating that flow structure development is highly sensitive to injection configuration and operating conditions (Bumrungthaichaichan & Wattananusorn 2019; Patwardhan 2003; Zughbi & Rakib 2004). Early studies primarily focused on isothermal mixing and momentum driven circulation, establishing key relationships between jet Reynolds number, penetration depth, and entrainment behaviour (Bumrungthaichaichan et al. 2016). Chi et al. (2023) and Kok et al. (2017) stated that in thermal systems, the coupling between fluid motion and heat transfer introduces additional complexity, as temperature gradients influence fluid properties and buoyancy effects can modify circulation patterns. Moreover, Oluwadero et al. (2023) revealed that the orientation of jet injection has been identified as a particularly important parameter, where axial jets tend to produce stronger bulk recirculation and deeper penetration, while side jets generate more localised, wall bounded flow structures. These differences directly affect temperature homogenization and cooling efficiency, highlighting the need for detailed analysis of hydrodynamic mechanisms in jet mixing for reactor thermal stability.

Computational Fluid Dynamics (CFD) has become an essential tool for investigating such complex thermo fluid phenomena, enabling detailed visualisation of velocity fields, temperature distributions, and turbulence characteristics (Thakur et al. 2022). By solving the governing equations of fluid flow and heat transfer, CFD provides mechanistic insight into the interaction between jet induced flow structures and thermal dissipation processes. Numerous studies have demonstrated that CFD can accurately predict reactor cooling behaviour when properly validated against experimental data, typically achieving deviations within a few percent (Bumrungthaichaichan 2016; Zughbi & Ahmad 2005). Nevertheless, transient CFD simulations remain computationally intensive, particularly when fine spatial and temporal resolution is required to capture the full evolution of cooling processes (Khan et al. 2021). This limitation restricts the feasibility of large-scale parametric studies and real time optimisation.

To overcome these challenges, artificial neural networks (ANN) have been increasingly adopted as data driven surrogate models capable of approximating complex nonlinear relationships in thermal fluid systems (Beigzadeh et al. 2025; Bhran et al. 2025). ANNs can be trained on CFD generated datasets to predict system behaviour with high accuracy and significantly reduced computational cost (Beigzadeh et al. 2025). Applications in thermal engineering have demonstrated their effectiveness in modelling heat transfer, optimising system performance, and enabling rapid design evaluation. However, the reliability of ANN predictions depends strongly on the quality of training data and the ability of the model to generalise beyond the sampled parameter space (Beigzadeh et al. 2025; Łach & Svyetlichnyy 2025). As such, the integration of experimental validation, CFD analysis, and ANN modelling have emerged as a powerful hybrid approach that influences the strengths of each method while mitigating their individual limitations.

Despite these advancements, existing studies often treat experimental, numerical and data-driven approaches in isolation. Limited attention has been given to the systematic investigation of transient cooling behaviour in jet mixing systems within stirrerless reactors. In particular, the relationship between hydrodynamic flow structures and time resolved thermal dissipation remains insufficiently understood, despite its importance for designing effective thermal runaway mitigation strategies (Kummer & Varga 2021; Wasewar 2006). Previous CFD-ANN studies have examined related mixing and cooling systems, such as multi-impeller mixing tanks (Beigzadeh et al. 2025) and synthetic jet cooling in microchannel heat sinks (Mohammadpour et al. 2022). However, these studies focused on impeller driven mixing and electronics scale cooling, rather than reactor scale continuous jet cooling for thermal runaway mitigation.

The present study addresses this gap by integrating experimental validation, transient CFD simulation and ANN surrogate modelling within a single framework. The specific objectives are to: (i) experimentally characterise cooling performance under different jet configurations; (ii) develop and validate a CFD model capable of resolving the underlying hydrodynamic and thermal processes; (iii) quantify cooling efficiency using appropriate performance

indicators, and (iv) construct an ANN based surrogate model for rapid prediction of system behaviour. By combining validated physical modelling with data driven prediction, this work provides both mechanistic understanding and practical tools for enhancing reactor safety, supporting the development of efficient, intelligent, and sustainable thermal management strategies in modern process industries.

METHODOLOGY

This study adopts an integrated experimental, computational and data-driven framework to investigate transient cooling performance in jet mixing reactor systems. The methodology combines controlled laboratory experiments, CFD simulation, and ANN surrogate modelling to provide both physical understanding and predictive capability.

EXPERIMENTAL INVESTIGATION

The experimental study was conducted using a cylindrical stainless-steel reactor vessel designed to investigate transient cooling behaviour under jet mixing conditions as shown in Figure 1. The reactor had a diameter of 0.16 m and a height of 0.24 m, corresponding to a fluid height-to-diameter ratio of 1.5. The vessel was equipped with jet injection nozzles to allow the evaluation of different jet configurations. Each nozzle had a diameter of 1/8 inch (0.0032 m). Two main jet configurations were investigated, namely N1 (90° axial bottom jet) and N2 (45° side jet). Water was used as the working fluid for both the hot bulk fluid and the injected cooling jet. The initial temperature of the reactor fluid was maintained at 355.45 K, while the injected cooling jet temperature was set at 305.25 K.

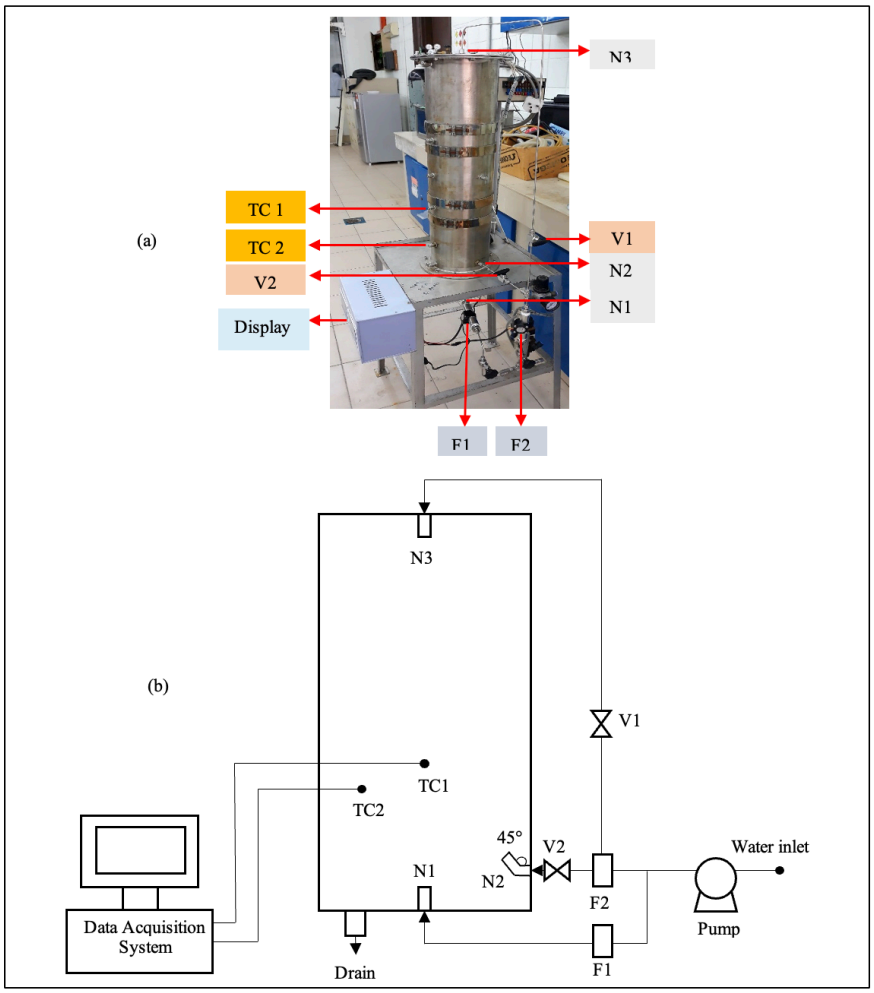


FIGURE 1. Experimental setup for thermal mixing investigation. (a) Photograph of the cylindrical reactor with instrumentation labels. (b) Schematic diagram showing the arrangement of nozzles (N1, N2, N3), thermocouples (TC1, TC2), flowmeters (F1, F2), valve (V1, V2), pump and data acquisition system.

Volumetric flow rates were controlled using calibrated flow meters to maintain consistent operating conditions across experiments. Temperature measurements were obtained using Type-K thermocouples (TC) installed at two fixed locations (TC1 and TC2) inside the reactor vessel to capture the spatial evolution of temperature during the cooling process. TC1 was positioned 0.226. m from the reactor base and 0.08 m from the reactor wall. TC2 was positioned 0.097 m from the reactor base and 0.035 m from the reactor wall. All temperature data were recorded using a real-time data acquisition system. These measurements also provided data for CFD validation at same temperature measurement position. It is to ensure a consistent basis of comparison between experimental and numerical results.

COMPUTATIONAL FLUID DYNAMICS (CFD) MODELING

THE GEOMETRIC MODEL

The computational model was developed using ANSYS 2025 R2 software to simulate the hydrodynamic flow structures and heat transfer mechanisms governing the transient cooling process within the reactor. A three-dimensional reactor geometry was constructed based on the dimensions of the experimental setup. The geometric model included the reactor vessel, jet injection nozzle, and drain outlet, ensuring accurate representation of the physical system. Table 1 shows the main parameters of the geometric model.

TABLE 1. Main parameters of the geometric model

Parameter	Values
Geometric height	0.24 m
Geometric diameter	0.16 m
Fluid height to reactor diameter ratio (H/D)	1.5
Nozzle diameter	0.0032 m
Drain diameter	0.0064 m

BOUNDARY CONDITIONS AND MESH INDEPENDENCE TEST

Table 2 shows the overview of simulation features and boundary conditions for the model. A tetrahedral meshes structure was employed, generated following the meshing procedures set out in the ANSYS Fluent User's Guide (ANSYS Inc., 2025b), to accurately resolve the complex flow behaviour inside the reactor as shown in Figure 2. To ensure numerical accuracy, a mesh independence test was conducted for the model (Taslin et al. 2021).

TABLE 2. Overview of simulation features and boundary conditions

Parameter	Conditions/Values
Geometry	3-dimensional
Models	Single-phase, Standard k-epsilon
Solver	Pressure-based, transient state
Solution method	SIMPLE
Inlet	Velocity calculated from volumetric flow rate (m/s)
Outlet	Pressure outlet
Reactor wall	Adiabatic wall
Top surface of the liquid	Symmetry boundary (zero shear wall)
Temperature of the fluid domain	355.45 K
Temperature of liquid jet	305.25 K
Jet angle	Side jet (5°, 25°, 45°, 65°) and axial jet (90° (bottom), 90° (top))

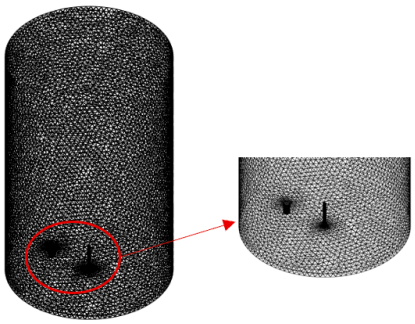


FIGURE 2. Mesh generation of the model

The velocity within the reactor was selected as the monitoring parameter. As shown in Figure 3, the solution exhibits noticeable variation at lower mesh densities but stabilises as the number of elements increases. Beyond approximately 298×10^3 elements, the variation in velocity becomes negligible, indicating mesh-independent behaviour. Therefore, the mesh with approximately 298×10^3 elements was selected for all subsequent simulations, providing an optimal balance between computational efficiency and solution accuracy.

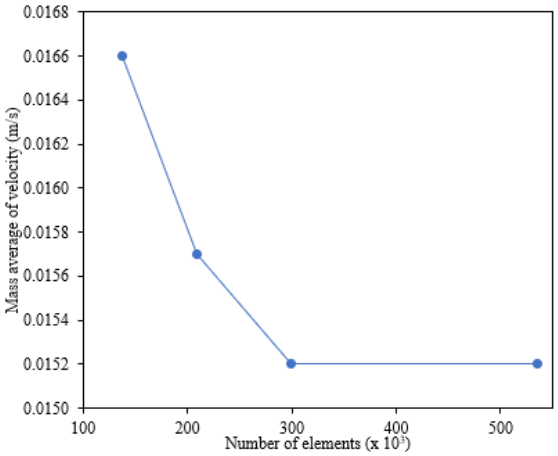


FIGURE 3. Mesh independence test of the model

GOVERNING EQUATION AND NUMERICAL METHOD

The governing equations solved in the CFD model include the continuity equation for mass conservation, the Navier–Stokes momentum equations, and the energy equation describing heat transport within the fluid domain as Equation 1-7.

(1) Continuity Equation

$$\frac{\partial u_i}{\partial x_i} = 0 \tag{1}$$

where u_i is the velocity component in the i-th direction, and x_i is the corresponding spatial coordinate.

(2) Momentum Equation

$$\frac{\partial(\rho u_i)}{\partial t} + \rho u_j \frac{\partial u_i}{\partial x_j} = -\frac{\partial p}{\partial x_i} + \frac{\partial}{\partial x_j}\left[\mu\left(\frac{\partial u_i}{\partial x_j} + \frac{\partial u_j}{\partial x_i}\right) - \rho u_i u_j\right] \tag{2}$$

where,

$$\rho u_i u_j = \mu_t\left(\frac{\partial u_i}{\partial x_j} + \frac{\partial u_j}{\partial x_i}\right) - \frac{2}{3}\delta_{ij}\rho k \tag{3}$$

In this equation, ρ is fluid density, p is pressure, μ and μ_t are the molecular and turbulent dynamic viscosities, δ_{ij} is the Kronecker delta, k is turbulent kinetic energy and t is time.

(3) Energy Equation

$$\frac{\partial(\rho T)}{\partial t} + \rho u_j \frac{\partial T}{\partial x_j} = \frac{\partial}{\partial x_j}\left[\left(\frac{\mu}{\sigma} + \frac{\mu_t}{\sigma_t}\right)\frac{\partial T}{\partial x_j}\right] \tag{4}$$

where T is temperature, σ and σ_t are the molecular and turbulent Prandtl number, respectively.

(4) Transport equation for k

$$\frac{\partial(\rho k)}{\partial t} + \rho u_j \frac{\partial k}{\partial x_j} = \frac{\partial}{\partial x_j}\left[\left(\mu + \frac{\mu_t}{\sigma_k}\right)\frac{\partial k}{\partial x_j}\right] + \mu_t\left(\frac{\partial u_i}{\partial x_j} + \frac{\partial u_j}{\partial x_i}\right)\frac{\partial u_j}{\partial x_i} - \rho\varepsilon \tag{5}$$

where σ_k is turbulent Prandtl number for k and ε is turbulent dissipation rate.

(5) Transport equation for ε

$$\frac{\partial(\rho\varepsilon)}{\partial t} + \rho u_j \frac{\partial \varepsilon}{\partial x_j} = \frac{\partial}{\partial x_j}\left[\left(\mu + \frac{\mu_t}{\sigma_\varepsilon}\right)\frac{\partial \varepsilon}{\partial x_j}\right] + C_{1\varepsilon}\frac{\varepsilon}{k}\mu_t\left(\frac{\partial u_i}{\partial x_j} + \frac{\partial u_j}{\partial x_i}\right)\frac{\partial u_j}{\partial x_i} - C_{2\varepsilon}\rho\frac{\varepsilon^2}{k} \tag{6}$$

where,

$$\mu_l = \rho C_\mu \frac{k^2}{\varepsilon} \tag{7}$$

In this equation, σ_ε is turbulent Prandtl number for ε and $C_{1\varepsilon}$, $C_{2\varepsilon}$ and C_μ are the constant. The closure coefficients appear in the equations are given by the following values: $C_{1\varepsilon}$=1.44, $C_{2\varepsilon}$=1.92, C_μ=0.09, σ_k=1.0, σ_ε=1.3.

Turbulence effects were modelled using the standard k–ε turbulence model, which is widely used for turbulent jet flows due to its numerical robustness and stability (Kabra et al. 2021; Zhu et al. 2021). The unsteady form of the governing equations adopted here, including the local time-derivative terms and the combined molecular and turbulent viscosity diffusion form, is consistent with the transport equations implemented in ANSYS Fluent (ANSYS Inc., 2025a).

A pressure-based transient solver was employed, with pressure–velocity coupling handled using the SIMPLE algorithm (Hasini & Zahari, 2025). Gradient calculations were performed using a least-squares cell-based approach, and second-order upwind discretisation schemes were applied to improve numerical accuracy. Transient simulations were performed to capture the temporal evolution of the cooling process. The time step of Δt=1*s* with 20 iterations per time step was used in the transient

simulation because the main physical process of interest is the macroscopic cooling behaviour. The estimated Courant number was approximately 293. Although this value is relatively high, the simulation was performed using fully implicit pressure-based formulation. In this approach, numerical stability is not strictly governed by the Courant-Friedrichs-Lewy (CFL) restriction commonly with explicit schemes (Bumrungthaichaichan 2016). Instead, the solution stability was assessed through residual convergence which were reduced below $1x10^{-6}$. Then, the temperature fields, velocity distributions, and volume-averaged cooling curves were extracted for further analysis.

The reactor wall was assumed to be adiabatic because external heat loss to the surroundings was considered negligible compared with the dominant forced convective cooling generated by the injected jet. When a high momentum jet is injected into the fluid, the rapid convective heat transfer and turbulent mixing completely dominate the energy transport within the vessel (Kumar & Halder 2024). This assumption is supported by the close agreement between experimental and simulation temperature decay in Table 3.

CFD MODEL VALIDATION

The CFD model was validated using experimental temperature measurements obtained during the cooling experiments. Temperature profiles predicted by the numerical simulations were compared with experimental data recorded at the same two probe locations within the reactor to assess the accuracy of the model. The comparison was performed by calculating the relative percentage error between the simulated and measured temperature values at six selected time of transient cooling period as shown in Table 3. The results showed that the relative percentage error between CFD predictions and experimental measurements remained consistently low, with an average error of approximately 1%. This close agreement indicates that the numerical model successfully captures the dominant hydrodynamic mixing and heat transfer mechanisms governing the cooling process. Therefore, the validated CFD framework can be considered reliable for analysing the influence of jet configuration on transient cooling performance within the reactor system.

TABLE 3. Relative percentage error of CFD simulation results with experimental data

Time (s)	Temperature (K)				Relative percentage error (%)	
	Experimental		CFD			
	Probe 1 (TC1)	Probe 2 (TC2)	Probe 1	Probe 2	Probe 1 (Exp vs CFD)	Probe 2 (Exp vs CFD)
30	355.05	355.05	348.15	350.56	1.94	1.26
300	333.05	333.45	329.66	331.19	1.02	0.68
600	320.45	321.75	318.78	319.71	0.52	0.64
900	315.95	316.15	312.80	313.35	1.00	0.89
1200	312.95	313.45	309.47	309.79	1.11	1.17
1380	311.45	312.55	308.23	308.46	1.03	1.31
Average					1.10	0.99

COOLING PERFORMANCE QUANTIFICATION

To quantitatively evaluate the effectiveness of the cooling process, the temperature evolution within the reactor was analysed using a normalised temperature parameter (θ). The normalised temperature is defined as Equation 8.

$$\theta = \frac{T - T_{cool}}{T_{initial} - T_{cool}} \quad (8)$$

where T is the instantaneous temperature, $T_{initial}$ is the initial reactor temperature, and T_{cool} is the temperature of the injected cooling jet. This normalisation allows the transient cooling behaviour to be compared consistently across different jet configurations and operating conditions by removing the influence of absolute temperature values. As the cooling process progresses, the normalised temperature decreases from θ = 1 (initial condition) toward values approaching zero as thermal equilibrium is approached. Two characteristic cooling indicators were extracted from the normalised temperature curves to quantify the transient cooling performance. The first indicator, t_{50}, represents the time required for the reactor to reach 50% temperature reduction relative to the initial thermal difference, corresponding to θ = 0.5. The second indicator, t_{90}, represents the time required to achieve 90% thermal homogenisation, corresponding to θ = 0.1. These parameters provide practical measures of cooling efficiency, where t_{50} reflects the early-to-intermediate cooling behaviour while t_{90} represents the long-term mixing and homogenisation stage of the cooling process.

ARTIFICIAL NEURAL NETWORK (ANN) MODELING

To complement the CFD analysis and enable rapid prediction of cooling performance, an ANN surrogate model was developed. The ANN was designed to learn the nonlinear relationship between jet configuration parameters and the resulting cooling behaviour obtained from the CFD simulations. By using CFD-generated data as the training dataset, the ANN model provides an efficient predictive tool capable of estimating cooling performance indicators without the need to perform repeated high-cost numerical simulations (Kalpana et al. 2024; Mohammadpour et al. 2022). Importantly, the ANN in this study was trained exclusively on CFD-generated data rather than direct experimental measurements. As a result, the network learns the input-output mapping of the computational model rather than the physical system itself. Since the baseline CFD model was validated against limited experimental temperature data (Table 3), the predictive accuracy of the resulting ANN surrogate fundamentally bounded by the fidelity of the underlying CFD model.

The ANN model adopted a feed-forward multilayer perception (MLP) architecture consisting of an input layer, hidden layer, and an output layer. Table 4 shows the initial ANN setting parameters. Three input variables included time, jet angle and jet position (side jet and axial jet), while the single output variables corresponded to the transient cooling temperature derived from the CFD results. To determine the optimal network structure, three hidden-layer configurations were tested containing 6, 8, and 10 neurons. The predictive performance of each architecture was evaluated using the mean squared error (MSE) between the predicted and target values. As jet position is a categorical variable, it was encoded as a binary indicator (0 for side jet, 1 for 90° axial bottom jet and 2 for 90° axial top jet) prior to input into the network. The continuous input variables (time and jet angle) were normalised to the range [0,1] using min-max scaling to ensure consistent input scaling across variables of differing magnitude (Beigzadeh et al. 2025).

TABLE 4. Initial ANN setting parameters

Parameter	Setting
Software	MATHLAB (Neural Network Fitting)
Number of datasets	3666 datasets; 70% training, 15% validation, 15% testing
Input layer	3
Number of neurons in the hidden layer	6, 8, 10
Output layer	1
Network type	A two-layer feed-forward network
Training algorithm	Levenberg-Marquardt
Hidden transfer function	Tangent sigmoid
Output transfer function	Purelin
Performance function	MSE, R

The dataset obtained from CFD simulations was divided into three subsets for model training and evaluation, consisting of 70% training data, 15% validation data, and 15% testing data. The training dataset was used to adjust the network weights during the learning process, while the validation dataset was used to monitor model generalisation and prevent overfitting. The testing dataset provided an independent evaluation of the final model performance. Network training was carried out using a Levenberg-Marquardt backpropagation learning algorithm implemented in MATLAB Neural Network Toolbox.

Model performance was assessed using mean squared error (MSE) and regression coefficient (R). A regression plot and error histogram were used to assess bias and distributional characteristics of prediction errors. The trained ANN model was further validated by comparing its predicted values of t_{50} and t_{90} with the corresponding CFD simulation results. The close agreement between ANN predictions and CFD outputs confirms that the surrogate model is capable of accurately reproducing the nonlinear cooling behaviour within the investigated parameter range. Consequently, the ANN model provides a computationally efficient tool for rapid evaluation and screening of jet configurations in reactor cooling applications.

RESULT AND DISCUSSION

TRANSIENT COOLING BEHAVIOUR UNDER DIFFERENT JET ARRANGEMENTS

Figure 4 presents the experimental transient evolution of the normalised temperature (θ) for two jet configurations, namely the 90° axial bottom jet injected from the bottom and the 45° side jet, at a Reynolds number of 4300. For

both configurations, the normalised temperature decreases steadily with time, indicating a progressive cooling process within the vessel. At the early stage of the transient period (60–120 s), the temperature values remain relatively high ($\theta \approx 0.9$–0.8) and the difference between the two jet arrangements is minimal. This suggests that the cooling behaviour during the initial phase is dominated by the immediate interaction between the injected cold jet and the surrounding fluid, resulting in comparable cooling rates for both configurations.

As the cooling process progresses to the intermediate and late stages (300–1380 s), a more noticeable difference between the two configurations becomes evident. The 90° axial bottom jet consistently produces slightly lower normalised temperature values compared to the 45° side jet, particularly at 300 s and beyond. This indicates that the axial jet arrangement promotes more effective heat removal over time.

At the final stage of the transient period, both configurations approach near-equilibrium conditions ($\theta \approx$ 0.1–0.2), although the axial jet maintains a marginally lower temperature throughout the process. The relatively small error bars observed across the measurements further indicate good experimental repeatability and reliability of the temperature data.

The experimental results indicated that jet orientation influences the effectiveness of transient cooling, particularly during the intermediate and late stages of the process. While both configurations exhibit similar behaviour at the early stage due to dominant local convective heat transfer near the jet impingement region. The differences observed at later times indicate that large-scale circulation and mixing patterns begin to govern the overall heat transfer performance. The axial jet injected from the bottom generates a stronger vertical recirculation flow that enhances the penetration of the cold fluid into the bulk region of the vessel. This trend agrees with previous CFD study, which reported the axial jets generate stronger core recirculation and deeper fluid penetration than side jets (Oluwadero et al. 2023; Torré et al. 2008).

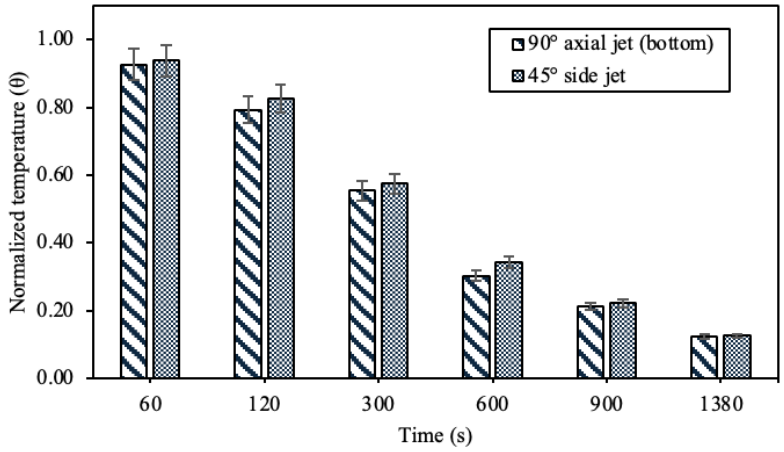


FIGURE 4. Experimental transient cooling distribution at Re 4300 for 45° side jet and 90° axial bottom jet

In contrast, the side jet configuration tends to produce more localised flow structures, which may limit the extent of mixing within the central region of the vessel. As a result, the redistribution of thermal energy throughout the fluid volume occurs at a slower rate compared to the axial injection configuration. This difference in flow behaviour explains the slightly higher normalised temperatures observed for the side jet during the intermediate and late stages of cooling. Therefore, the improved performance of the axial jet can be attributed to its ability to induce stronger bulk circulation and reduce thermal stratification within the reactor.

Figure 5 presents the transient decay of normalised temperature (θ) for six different jet configurations, including side jets at 5°, 25°, 45°, and 65°, as well as axial jets at 90° injected from the bottom and top of the vessel. For all configurations, the normalised temperature decreases monotonically from $\theta = 1$ toward near-zero values as time progresses, indicating effective cooling throughout the transient period.

During the early stage of cooling ($t < 400$ s), the temperature profiles for all configurations showed minor variations between different jet orientations. This indicates that the initial cooling behaviour is largely similar regardless of jet angle, with temperature dropping rapidly as the injected cold fluid begins interacting with the surrounding bulk fluid.

As the cooling process progresses into the intermediate

and late stages (t > 600 s), clearer separation among the temperature curves becomes visible. The 90° axial jet injected from the top side consistently exhibits the lowest normalised temperature values, indicating the fastest cooling behaviour among all configurations. Conversely, the 5° side jet maintains the highest temperature profile over time, suggesting slower heat removal. The remaining configurations (25°, 45°, and 65° side jets as well as the 90° axial bottom jet) fall between these two extremes. The dashed horizontal lines marking t_{50} (θ = 0.5) and t_{90} (θ = 0.1) further highlight the differences in cooling performance, where higher-angle jet configurations generally intersect these thresholds earlier than lower-angle jets.

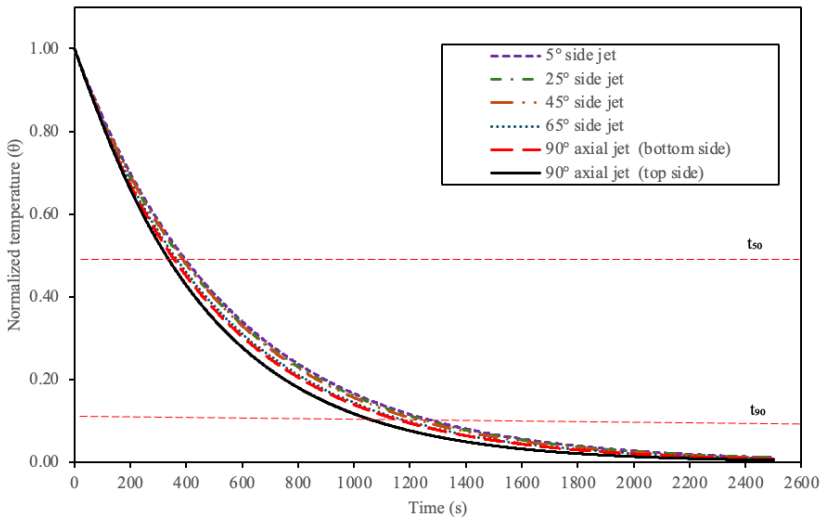


FIGURE 5. CFD transient cooling distribution at Re 4300 for different jet configurations

From a thermal mixing and reactor design perspective, the results demonstrate that jet orientation plays a critical role in controlling transient heat removal efficiency as investigated by Parvareh et al. (2009). The superior performance of the 90° axial top jet suggests that directing the cooling fluid vertically into the vessel can create more effective global circulation loops, which facilitate the rapid transport of heat from the warmer fluid regions to the cooling jet. Such circulation patterns promote more uniform temperature distribution and reduce the persistence of thermal stratification within the vessel.

These findings highlight the importance of optimising jet placement and injection angle in cooling system design for reactors or mixing vessels handling heat-sensitive processes. Even though all configurations eventually reach similar final temperatures, the time required to achieve significant cooling differs noticeably among them. By selecting jet orientations that enhance bulk mixing such as axial injection, engineers can improve cooling efficiency, shorten transient thermal response times, and enhance the safety and stability of thermally reactive systems.

FLOW AND THERMAL DISTRIBUTIONS ANALYSIS

EVOLUTION OF COOLING PHASES

Figure 6 illustrates the temporal evolution of the normalised temperature (θ) during the cooling process, highlighting three distinct stages: the initial phase, the fast transient cooling phase, and the asymptotic phase. At the beginning of the process of 1 s, the injected cooling jet interacts locally with the surrounding hot fluid, creating a small region of temperature disturbance near the injection point. The overall temperature field remains largely unchanged in the bulk region, indicating that large-scale mixing has not yet developed. As time progresses to approximately 200 s, the cooling process enters the fast transient phase, where the temperature distribution begins to change more significantly and larger circulation structures become visible. By 1000 s, the temperature field becomes more uniformly distributed, and the cooling curve starts to flatten. At later times such as 1500 s, the system approaches thermal equilibrium, with the normalised temperature decreasing gradually and the remaining temperature gradients becoming minimal.

The observed behaviour indicates that the cooling process is governed by the development of flow circulation and mixing intensity over time as proven by Zughbi (2006). During the initial phase, the cooling effect is limited to the vicinity of the jet outlet because the injected fluid has not yet penetrated the entire vessel. As the jet momentum induces stronger recirculation patterns, the system transitions into the fast transient cooling phase, where the interaction between the cooling jet and the bulk fluid significantly enhances convective heat transfer. This stage is characterised by rapid temperature reduction due to efficient mixing and redistribution of thermal energy. Eventually, the cooling rate decreases as the process enters the asymptotic phase, where most of the fluid has already been cooled and the remaining temperature gradients become smaller. At this stage, heat transfer is dominated by slower mixing processes and the gradual elimination of residual thermal pockets within the vessel.

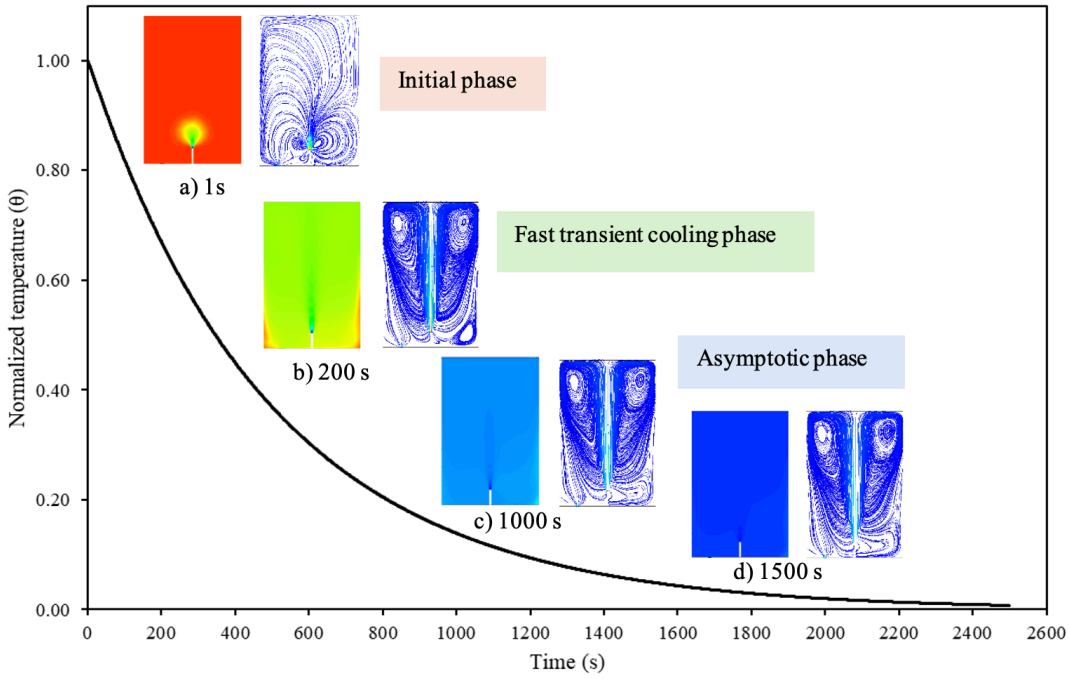


FIGURE 6. Transient cooling process of the reactor

FLOW AND TEMPERATURE DISTRIBUTION FOR DIFFERENT JET CONFIGURATIONS

The spatial evolution of temperature and flow structures was further examined to understand how jet orientation influences mixing and heat transport within the vessel. Representative temperature contours and velocity streamlines are presented for three jet configurations: 5° side jet, 45° side jet, and 90° axial jet injected from the top, at different time instances during the cooling process. These visualisations provide insight into the development of circulation patterns and their role in redistributing thermal energy throughout the fluid domain. By comparing the temperature fields and corresponding velocity structures, the influence of jet angle on mixing intensity and cooling effectiveness can be more clearly interpreted

The temperature contours in Figure 7 reveal the progressive cooling behaviour for the three representative jet configurations at 60 s, 600 s, and 1000 s. At the early stage (60 s), the temperature distribution remains relatively high throughout the vessel for all configurations, indicating that the cooling effect is initially localised near the jet injection region. For the 5° side jet, the cooling influence appears concentrated near the lower side region where the jet enters, while most of the vessel retains higher temperatures. The 45° side jet exhibits a slightly broader cooling region, suggesting stronger interaction between the injected fluid and the surrounding bulk fluid. In contrast, the 90° axial top jet shows a more symmetric temperature distribution, with the cooler fluid penetrating vertically into the central region of the vessel.

As the cooling process progresses to 600 s and 1000 s, the temperature becomes increasingly uniform for all cases, reflecting the continued redistribution of thermal energy within the vessel. However, noticeable differences remain between the configurations. The 5° side jet still exhibits weaker penetration of the cooling fluid toward the central region, whereas the 45° side jet produces a broader cooling zone due to enhanced mixing. The 90° axial top jet demonstrates the most uniform temperature distribution

across the vessel at later stages. The velocity streamline patterns further highlight these differences, where the 5° configuration produces a relatively asymmetric circulation structure, the 45° configuration generates stronger recirculating vortices, and the 90° axial top jet forms a more symmetric and vertically oriented flow pattern.

The observed temperature distributions and streamline structures indicate that jet orientation significantly influences the development of circulation patterns and mixing intensity within the vessel (Bumrungthaichaichan et al. 2016; Oluwadero et al. 2023). For the 5° side jet, the jet momentum is primarily directed along the vessel wall, which restricts the penetration of the cooling fluid into the central region of the vessel. As a result, the redistribution of thermal energy occurs more slowly and the cooling process is less effective. Increasing the injection angle to 45° improves the interaction between the jet and the surrounding fluid, producing stronger recirculation zones that enhance convective heat transfer within the vessel.

In contrast, the 90° axial top jet generates a vertically driven circulation pattern that facilitates efficient mixing across the entire fluid domain. The injected fluid moves downward into the vessel before recirculating upward along the vessel walls, forming large-scale symmetric vortices. This circulation structure enables the cooling fluid to penetrate deeper into the bulk region and promotes more effective heat redistribution, explaining the more uniform temperature distribution observed for the axial configuration at later times (Torré et al. 2008; Zughbi & Ahmad 2005).

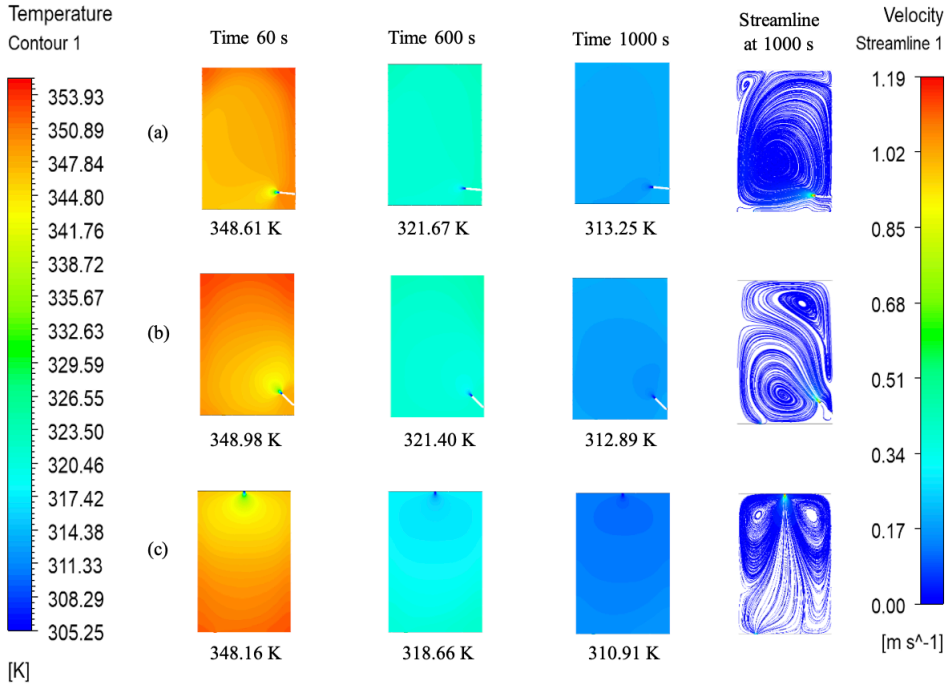


FIGURE 7. Flow and temperature distribution for (a) 5° side jet, (b) 45° side jet and (c) 90° axial top jet

These results highlight the importance of optimising jet orientation in cooling system design for mixing vessels and reactor applications. Even though all configurations eventually approach similar final temperature levels, the path toward thermal equilibrium differs significantly depending on the flow structures generated by the jet. Configurations that enhance circulation and fluid entrainment, such as the 90° axial injection, can significantly improve thermal homogenization and reduce the time required to achieve effective cooling.

QUANTITATIVE COOLING PERFORMANCE INDICATORS (t_{50} AND t_{90})

Table 5 presents the quantitative cooling performance indicators for the six jet configurations evaluated in this study. The results show a clear variation in cooling time depending on jet orientation. The 5° side jet exhibits the longest cooling times with t_{50} = 381 s and t_{90} = 1254 s, ranking last among all configurations. As the jet angle increases from 25° to 65°, both t_{50} and t_{90} gradually decrease, indicating improved cooling performance. The 65° side jet achieves t_{50} = 351 s and t_{90} = 1163 s, representing the best performance among the side jet configurations.

The axial jet configurations further improve cooling performance, where the 90° axial bottom jet achieves t_{50} = 342 s and t_{90} = 1145 s.

Among all configurations, the 90° axial top jet demonstrates the fastest cooling behaviour, with t_{50} = 325 s and t_{90} = 1051 s, ranking first for both indicators. Compared to the worst-performing configuration (5° side jet), the axial top jet reduces t_{50} by approximately 56 s (14.7%) and t_{90} by 203 s (16.2%). These results indicate that higher jet angles and axial injection arrangements lead to shorter cooling times and improved thermal homogenisation within the vessel.

TABLE 5. Quantitative cooling performance indicators for different jet configurations

Jet configuration	Angle (°)	t_{50} (s)	t_{90} (s)	Rank by t_{50}	Rank by t_{90}
Side jet	5	381	1254	6	6
Side jet	25	370	1234	4	5
Side jet	45	372	1212	5	4
Side jet	65	351	1163	3	3
Axial jet (bottom)	90	342	1145	2	2
Axial jet (top)	90	325	1051	1	1

The quantitative results suggest that jet orientation plays a significant role in determining the efficiency of transient cooling. Lower-angle side jets such as the 5° configuration direct the injected fluid primarily along the vessel wall, which limits the penetration of the cooling jet into the central region of the vessel. This results in weaker mixing and slower redistribution of thermal energy, leading to longer cooling times.

The transition from side jet configurations to axial jets further enhances this mixing behaviour. The 90° axial jets introduce the cooling fluid directly into the central region of the vessel, creating stronger recirculation patterns that facilitate more efficient heat transfer. The superior performance of the top axial jet indicates that this configuration promotes more effective global circulation and improved mixing compared to the bottom injection configuration (Patwardhan, 2003).

CFD-ANN HYBRID ANALYSIS

The performance of the artificial neural network (ANN) model was evaluated using different hidden layer sizes, namely 6, 8, and 10 neurons, as summarised in Table 6. The results indicate that the prediction accuracy improves significantly when the number of neurons increases from 6 to 8. The 8-neurons configuration produces the smallest mean squared error (MSE) values.

TABLE 6. Mean squared error of training, validation and testing for different number of hidden layers

Neurons	Training MSE	Validation MSE	Testing MSE	Overall Quality
6 neurons	6.42×10^{-6}	6.44×10^{-6}	5.9×10^{-6}	Good
8 neurons	7.67×10^{-8}	7.84×10^{-8}	6.22×10^{-8}	Excellent
10 neurons	9.61×10^{-8}	7.22×10^{-8}	7.33×10^{-8}	Very good

This result indicates that the 8-neuron architecture effectively captures the relationship between the input parameters and the cooling performance indicators. It also supports the use of the ANN models as surrogate tool for complex thermal fluid simulations (Beigzadeh et al. 2025; Waqas et al. 2026). The main advantage of this approach is the reduction in computational time. While each transient CFD simulation requires substantial computational effort (requiring several hours to complete), the trained ANN can predict t_{50} and t_{90} within milliseconds. This allows rapid parametric screening of jet configurations that would be difficult to achieve using CFD alone.

The training performance of the ANN model is illustrated in Figure 8(a), which presents the evolution of the mean squared error (MSE) during the learning process. The MSE decreases rapidly during the early training stages, indicating that the network quickly captures the dominant relationships between the input variables and the target outputs. As the training progresses, the reduction in error becomes more gradual and eventually stabilises after approximately 750 epochs, reaching a final value on the order of 10^{-8}. The training, validation, and testing curves closely follow each other throughout the learning process, suggesting that the network maintains consistent

performance across all datasets. This behaviour indicates that the model successfully converges during training and that the learning process remains stable without significant divergence or oscillation in prediction error.

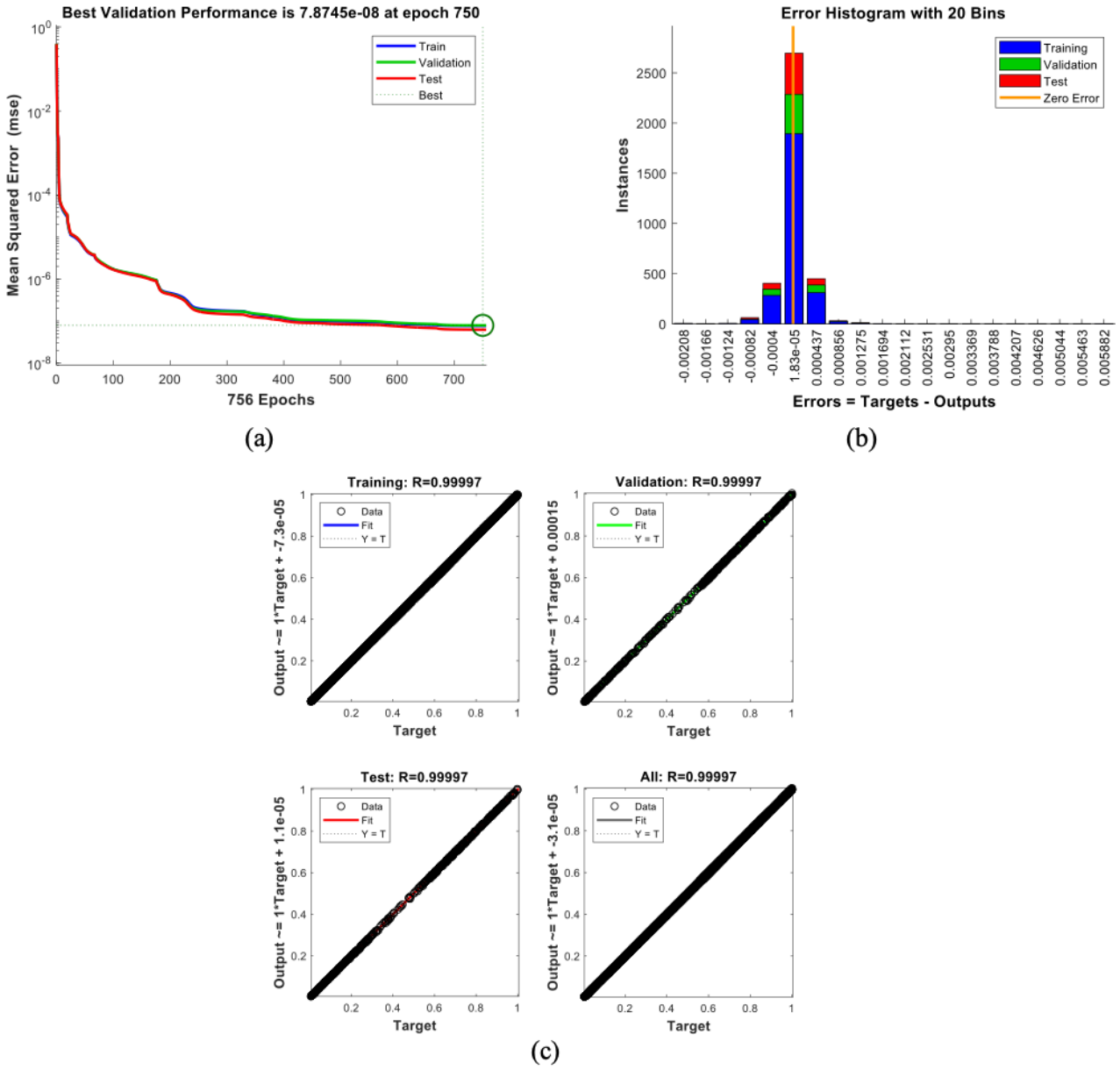


FIGURE 8. ANN model performance. (a) Mean squared error. (b) Error histogram. (c) Regression plot.

The error histogram shown in Figure 8(b) further confirms the accuracy of the trained ANN model. The distribution of prediction errors is strongly concentrated around the zero-error region, with only a small spread of values across the training, validation, and testing datasets. Most of the prediction errors fall within a narrow range near zero, indicating that the ANN predictions closely match the corresponding CFD-generated target values.

The regression plots presented in Figure 8(c) provide additional validation of the ANN model by comparing the predicted outputs with the target CFD values. The regression results show that the predicted outputs closely align with the reference y = x line, indicating a strong correlation between the ANN predictions and the CFD data. These results also demonstrate that the trained ANN model achieves high prediction accuracy, supporting its application as a rapid predictive tool for transient jet mixing cooling performance.

Table 7 shows the comparison between CFD-derived cooling time indicators and ANN-predicted values for

representative jet configurations at both t_{50} and t_{90}. The results show a consistently close agreement between CFD and ANN predictions across all configurations. The percentage errors within approximately 1.31% to 2%, indicating very high prediction accuracy. Overall, these results confirm that the ANN model successfully captures the nonlinear mapping between jet configuration and cooling performance.

TABLE 7. Comparison of CFD and ANN result at t_{50} and t_{90} for 5° side jet, 45° side jet and 90° axial jet (top)

	5° side jet			45° side jet			90° axial jet (top)		
	CFD (s)	ANN (s)	Percentage error (%)	CFD (s)	ANN (s)	Percentage error (%)	CFD (s)	ANN (s)	Percentage error (%)
Time at 50% mixing (t_{50})	381	376	1.31	372	367	1.34	325	320	1.54
Time at 90% mixing (t_{90})	1254	1229	1.99	1212	1188	1.98	1051	1030	2.00

The consistency of low errors across different jet arrangements also indicates that the model generalises well within the studied parameter space and not biased toward a specific configuration. Therefore, integration of CFD and ANN provides a robust hybrid framework that combines physical fidelity with computational efficiency, enabling fast and reliable prediction of cooling performance for thermal runaway prevention strategies.

CONCLUSION

This study presents an integrated experimental and hybrid CFD–ANN analysis of transient cooling behaviour in jet mixing systems. The results demonstrate that jet orientation significantly influences cooling performance, where axial injections consistently achieve faster thermal decay compared to side jet configurations. The 90° axial top jet shows the best performance, reducing cooling times and enhancing thermal homogenization. Hence, improving the system's ability to suppress temperature gradients that may trigger thermal instability.

From a hydrodynamic perspective, CFD analysis reveals that axial jets generate strong, symmetric recirculation structures that promote effective bulk mixing and rapid heat redistribution. In contrast, side jets produce localised and asymmetric flow patterns that limit penetration and delay cooling. These findings confirm that reactor thermal stability is strongly governed by flow structure development during transient cooling, rather than solely by operating conditions.

The ANN model successfully captured the nonlinear relationship between jet configuration and cooling performance indicators. Its predictions were consistent with the CFD derived trends, showing that the model can reproduce the main cooling behaviour obtained from the simulations. Beyond its low prediction error, the ANN provides a rapid surrogate tool for preliminary screening of jet configurations without requiring repeated transient CFD simulations. However, the model should be considered as a complementary tool to CFD, since detailed hydrodynamic features such as recirculation, entrainment, and vortex formation still require flow field analysis. Overall, the integrated experimental, CFD and ANN approach supports faster evaluation of jet mixing designs for enhancing heat removal and improving reactor thermal stability under transient cooling conditions.

ACKNOWLEDGEMENT

The authors would like to acknowledge the support of Universiti Teknologi MARA, Shah Alam, Selangor, Malaysia, and Faculty of Engineering and Built Environment, Universiti Kebangsaan Malaysia, Bangi, Selangor for providing the facilities on this research.

DECLARATION OF COMPETING INTEREST

None.

REFERENCES

ANSYS Inc. 2025a. *ANSYS Fluent Theory Guide, Release 2025 R2*. Canonsburg, PA: ANSYS Inc.

ANSYS Inc. 2025b. *ANSYS Fluent User's Guide, Release 2025 R2*. Canonsburg, PA: ANSYS Inc.

Balasubramanian, S. G., Dakshinamoorthy, D., & Louvar, J. F. 2003. Shortstopping runaway reactions. *Process Safety Progress* 22(4): 245-251.

Beigzadeh, R., Soltanian, S. & Azizpour, Y. 2025. Enhancing mixing efficiency in multi-impeller tanks

through innovative CFD and artificial neural network approaches. *Results in Engineering* 27:106594.

Bhran, A.A., Maghrabie, H.M., Gadallah, A. & Fawaz, H.E. 2025. Experimental investigation and ANN-based prediction of average Nusselt number for a flat surface subjected to double inclined air jets. *Scientific Reports* 15(1):37738.

Bumrungthaichaichan, E. 2016. A review on numerical consideration for computational fluid dynamics modeling of jet mixing tanks. *Korean Journal of Chemical Engineering* 33(11): 3050–3068.

Bumrungthaichaichan, E., Jaiklom, N., Namkanisorn, A. & Wattananusorn, S. 2016. On the computational fluid dynamics (CFD) analysis of the effect of jet nozzle angle on mixing time for various liquid heights. *Scientific Research and Essays* 11(4): 42–56.

Bumrungthaichaichan, E. & Wattananusorn, S. 2019. CFD modelling of pump-around jet mixing tanks: a reliable model for overall mixing time prediction. *Journal of the Chinese Institute of Engineers* 42(5): 428–437.

Chen, Q., Ni, L., Jiang, J. & Wang, Q. 2021. Modelling of runaway inhibition in batch reactors using encapsulated phase change materials. *Renewable Energy* 170: 387–399.

Chen, Q., Wang, J., Gao, M., Liu, L. & Tao, J. 2022. Review on loss prevention of chemical reaction thermal runaway: Principles and application. *Emergency Management Science and Technology* 2(1): 1–8.

Chi, X., Dong, P. & Wang, N. 2023. Numerical investigation of the fluid retention in the tank with a horizontal negatively buoyant jet. *Progress in Nuclear Energy* 156:104558.

Dakshinamoorthy, D., Khopkar, A.R., Louvar, J.F. & Ranade, V. V. 2006. CFD simulation of shortstopping runaway reactions in vessels agitated with impellers and jets. *Journal of Loss Prevention in the Process Industries* 19(6):570-581.

Hasini, H. & Zahari, M.F.Z.I.C. 2025. CFD Analysis of flow and swirl formation in tangential-type furnace. *Jurnal Kejuruteraan* 37(8): 3673–3689.

Kabra, A., Nema, A., Karvinkoppa, M., Nema, A. & Thorat, S. 2021. Computational fluid dynamics used by mixing vessels for predicting hydrodynamic behaviour of mixture: An overview. *Materials Today: Proceedings* 47:2305–2309.

Kalpana, V., Sujana, G.J., Thyagarajan, K., Lalitha, R.V.S., Talasila, V. & Jadhav, M.M. 2024. Enhancing heat transfer coefficient predictions in complex geometries through hybrid machine learning approaches. *Thermal Science and Engineering Progress* 55:103017.

Khan, S.A., Ibrahim, O.M. & Aabid, A. 2021. CFD analysis of compressible flows in a convergent-divergent nozzle. *Materials Today: Proceedings* 46:2835–2842.

Kok, B., Varol, Y., Ayhan, H. & Oztop, H.F. 2017. Experimental and computational analysis of thermal mixing characteristics of a coaxial jet. *Experimental Thermal and Fluid Science* 82: 276–286.

Kumar, S., & Halder, P. 2024. Thermal performance analysis of twin pulsating turbulent jets impinging over intermittently moving plate. *Arabian Journal for Science and Engineering* 49(8):10387-10408.

Kummer, A. & Varga, T. 2021. What do we know already about reactor runaway? – A review. *Process Safety and Environmental Protection* 147:460-476.

Łach, Ł. & Svyetlichnyy, D. 2025. Advances in numerical modelling for heat transfer and thermal management: A review of computational approaches and environmental impacts. *Energies* 18(5):1302.

Liu, G. & Wilhite, B.A. 2022. Development of compartment model for inhibition of thermal runaway in free-radical polymerization. *Chemical Engineering Science* 258:117758.

Mohammadpour, J., Husain, S., Salehi, F. & Lee, A. 2022. Machine learning regression-CFD models for the nanofluid heat transfer of a microchannel heat sink with double synthetic jets. *International Communications in Heat and Mass Transfer* 130:105808.

Oluwadero, T.A., Xuereb, C., Aubin, J. & Poux, M. 2023. Effect of jet nozzle position on mixing time in large tanks. *Processes* 11(7):2200.

Parvareh, A., Rahimi, M. A. S. O. U. D., & Abdulaziz Alsairafi, A. (2009). Experimental and CFD studies on the effect of the jet position on mixing performance. *Iranian Journal of Chemical Engineering (IJChE)* 6(3):3-12.

Patwardhan, A. W., & Gaikwad, S. G. 2003. Mixing in tanks agitated by jets. *Chemical Engineering Research and Design* 81(2): 211-220.

Rossi, F., Copelli, S., Colombo, A., Pirola, C. & Manenti, F. 2015. Online model-based optimization and control for the combined optimal operation and runaway prediction and prevention in (fed-)batch systems. *Chemical Engineering Science* 138: 760–771.

Taslin, P.N.A., Albani, A., Ibrahim, M.Z., Musa, M.A., Mohd Yusop, Z. & Jusoh, M.A. 2021. Computational fluid dynamics analysis of seven selected hydrofoils for different angle of attack. *Jurnal Kejuruteraan* 1:71–75.

Thakur, A.K., Kumar, R., Banerjee, N., Chaudhari, P. & Gaurav, G.K. 2022. Hydrodynamic modelling of liquid-solid flow in polyolefin slurry reactors using CFD techniques – A critical analysis. *Powder Technology* 405: 117544.

Torré, J.P., Fletcher, D.F., Lasuye, T. & Xuereb, C. 2007. Transient hydrodynamics and free surface capture of an under-baffled stirred tank during stopping. *Chemical Engineering Research and Design* 85(5):626–636.

Torré, J.P., Fletcher, D.F., Lasuye, T. & Xuereb, C. 2008. An experimental and CFD study of liquid jet injection into a partially baffled mixing vessel: A contribution to process safety by improving the quenching of runaway reactions. *Chemical Engineering Science* 63(4):924–942.

Waqas, H., Khan, M.A., Hussain, M. & Liu, S. 2026. Enhancing thermal performance in latent heat storage systems: A comparative study of CFD and ANN with nano-integrated phase change material. *International Communications in Heat and Mass Transfer* 172:110447.

Wasewar, K.L. 2006. A design of jet mixed tank. *Chemical and Biochemical Engineering Quarterly* 20(1):31–46.

Yang, D., Ni, L., Gu, L., Chen, Q., Jiang, J. & Su, J. 2024. Temperature control for the synthesis of n-butylmagnesium bromide Grignard reagent based on n-octadecane/polystyrene microPCMs. *Journal of Loss Prevention in the Process Industries* 89:105320.

Zhu, J., Frerich, T. & Herrmann, A.S. 2021. CFD modelling and validation of heat transfer inside an autoclave based on a mesh independency study. *Journal of Composite Materials* 55(18):2469–2487.

Zughbi, H. D. 2006. Numerical simulation of mixing in a jet agitated horizontal cylindrical tank. *International Journal of Computational Fluid Dynamics* 20(2):127-136.

Zughbi, H.D. & Ahmad, I. 2005. Mixing in liquid-jet-agitated tanks: Effects of jet asymmetry. *Industrial and Engineering Chemistry Research* 44(4):1052–1066

Zughbi, H.D. & Rakib, M.A. 2004. Mixing in a fluid jet agitated tank: Effects of jet angle and elevation and number of jets. *Chemical Engineering Science* 59(4): 829–842.